

Review on some Stefan Problems for Particle Dissolution in Solid Metallic Alloys

F. J. Vermolen¹, C. Vuik¹, E. Javierre¹, S. van der Zwaag²

¹ Delft Institute of Applied Mathematics

² Department of Aerospace Engineering, Delft University of Technology
The Netherlands

Received: 22.07.2005

Accepted: 31.08.2005

Abstract. This paper is a review of a suite of mathematical models of increasing complexity on particle dissolution in metallic alloys. This work deals with models for multi-component particle dissolution in multi-component alloys, where various chemical species diffuse simultaneously, and a two-dimensional model incorporating interfacial reactions as in the model of Nolfi [1]. The work is mathematically rigorous where asymptotic solutions and solution bounds are derived but is also of a practical nature as particle dissolution kinetics is modelled for industrially relevant conditions.

Keywords: particle dissolution, Stefan problem, diffusion, moving grid method, level-set method.

1 Introduction

1.1 Technological background

In the thermal processing of both ferrous and non-ferrous alloys, homogenization of the existing microstructure by annealing at such a high temperature that unwanted precipitates are fully dissolved, is required to obtain a microstructure suited to undergo heavy plastic deformation as well as providing an optimal starting condition for a subsequent precipitation hardening treatment. Such a homogenization treatment is for example applied prior to hot-rolling of Al killed construction steels, HSLA steels, all engineering steels, as well as in processing aluminium extrusion alloys. Although precipitate dissolution is not the only

metallurgical process taking place during homogenization, it is often the most critical of the processes occurring. The minimum temperature at which the annealing should take place can be determined from thermodynamic analysis of the phases present. However, the minimum annealing time at this temperature is not a constant but depends on particle size, particle geometry, particle concentration, overall composition etc. To make the homogenization treatment more efficient, it is highly desirable to have robust physical models for the kinetics of particle dissolution as a function of thermodynamics and thermokinetics data as well as particle morphology and microstructural dimensions. Using such models the minimum annealing times and optimum heating strategies can be calculated a priori, rather than be determined experimentally, and at great cost.

Apart from their technological relevance, accurate physical models for particle dissolution are, due to the complexity of the processes, also of great scientific and mathematical interest in themselves.

1.2 Existing models for particle dissolution

To describe particle dissolution several older mathematical models have been developed, which incorporate long-range diffusion [2–4] and non-equilibrium conditions at the interface [1, 5]. In general, the dissolution of particles proceeds via decomposition of the chemical compound, the crossing of the atoms of the interface and long-range diffusion in the matrix. The first two processes are referred to as the interfacial processes. The long-range diffusion models are based on the assumption that the interfacial processes are infinitely fast. Hence, these models provide an upper boundary for the dissolution kinetics.

The first models were based on analytical solutions for the interfacial position as a function of time (see for instance Whelan [2] and Crank [6]). However, in these solutions the volume in which dissolution takes place is infinite. As far as we know, Baty, Tanzilli and Heckel were the first authors in the metallurgical community to apply a Finite Difference Model [3] where the volume is bounded. Tundal and Ryum [4] also applied a Finite Difference Model in which a lognormal particle size distribution is included. They showed that the macroscopic dissolution rates depend strongly on the particle size and possible interactions between subsequent particles. Nolfi's [1] model was, as far as known, the first model in which

non-equilibrium conditions at the particle-matrix interface were included. However, the interface migration was not included. The non-equilibrium condition is modelled by a Robin-condition at the interface. Their solution is in terms of a Fourier series. Aaron and Kotler [5] combine Whelan's solution with the incorporation of the Gibbs-Thomson effect to deal with the influence of curvature on the interface motion. Further, they transform the Robin-boundary condition of Nolfi's model into a Dirichlet boundary condition. Recently, Svoboda *et al* [7] analyzed the kinetics of diffusional transformations where mechanical and chemical forces exerted on interfaces between subsequent phases are incorporated. Their approach is based on thermodynamical concepts that can be found in Hillert [8]. They obtain a thermodynamically based procedure to predict non-equilibrium interface kinetics by using both analytical and numerical techniques.

However, all these mentioned models did not consider the technologically important dissolution of multi-component particles in multi-component alloys. As far as we know Ågren *et al* [9] was the first to extend the models to multi-component alloys. His formalism was based on a thermodynamic treatment of diffusion in terms of chemical potentials and an interface motion from a material balance. The numerical methods that were used by Ågren were improved by Crusius *et al* [10] and the diffusion model was improved in [11], which forms the backbone of the software-package DICTRA suitable for dissolution and growth problems with one spatial dimension. The thermodynamic relation, which defined the boundary conditions at the moving interface, was simplified to a hyperbolic relationship. This has been done for iron-based alloys by Vitek *et al* [12] and Hubert [13]. Furthermore, Reiso *et al* [14] investigated the dissolution of Mg_2Si alloys in aluminium alloys by the use of the same principles.

The above mentioned authors viewed particle dissolution as a Stefan problem: a diffusion equation with a sharp moving interface. A recent approach is the phase-field approach, which is derived from a minimization of the energy functional and based on a diffuse interface between the consecutive phases. This approach has, among others, been used by Kobayashi *et al* [15] and Burman *et al* [16] to simulate dendritic growth. An extension to multi-component phase-field computation is done by Grafe *et al* [17], where solidification and solid-state transformation is modelled. For the one-dimensional case they obtain a perfect

agreement between the phase-field approach and the software package DICTRA, which is based on a sharp interface between the consecutive phases. Furthermore, some recent comparison studies of phase-field with a Stefan problem, solved by a moving mesh method or a level-set method or a mesh-free method, were done by Javierre *et al* [18] and Kovacevic and Sarler [19] respectively. Some disadvantages of the phase-field approach are that (1) no simple quick estimation of the solution is available, and that (2) physically justifiable parameters in the energy functional are not easy to obtain. Generally those parameters are to be obtained from fitting procedures that link experiment, thermodynamic data-bases and numerical computation. An other disadvantage of the phase-field is the requirement of a fine grid resolution in the diffuse interface region in order to have agreement with the solution of the “sharp interface problem”. This poses a severe time-step criterion and hence time consuming computations. This was observed by Burman *et al* [16] and Javierre *et al* [18]. Therefore, we limit ourselves here to viewing particle dissolution as a (vector) Stefan problem. We remark that Thornton *et al* [20] wrote a nice review paper on simulating diffusional phase transformations using several physical model approaches as the updated thermodynamic methods by Ågren, used in the package DICTRA, and the diffuse interface phase-field and (Allen)-Cahn-(Hilliard) approach. Thornton *et al* [20] also describe several two-dimensional applications of phase coarsening with Ostwald Ripening using the diffuse interface approach. The present review paper will focus on the computational aspects of solving Stefan problems with a sharp interface applied to particle dissolution in (multi-component) alloys. Furthermore, some mathematical issues will be summarized.

Although much work on the mathematical modeling of dissolution of particles had been done, some major limitations remained (until recently):

1. No fast and efficient numerical method for the simultaneous dissolution of a particle and a segregation at the grain boundary was available. Furthermore, no quick and well motivated self-similar solution for the dissolution of particles in multi-component has been reported.
2. Some particles may be disk-shaped, hence a two-dimensional model is necessary to compute the dissolution of the particle. With the classical literature of Finite Elements the computation of the interface movement with a sharp

angle within the boundary is impossible. Furthermore, the case where two particles dissolve in one cell needs to be discussed.

3. No numerical model, be it 2D or quasi 3D, that treats the interface movement while the interfacial reactions take place exists.
4. Metallurgical experiments on alloys indicate that dissolving particles or phases may break up into smaller particles or phases in some circumstances. No metallurgically sound model in three spatial dimensions, based on the sharp interface approach, exists to deal with these topological changes.

These limitations were lifted in a suite of mathematical models of increasing complexity. This paper presents a coherent total picture of the basic concepts and equations in these models and illustrates their potential.

Furthermore, an experimental validation of the above mentioned models can be found in [21] and [22]. In the first paper the activation energy for particle dissolution has been analyzed. In the second paper the experimental validation was carried out using DSC-measurements. New work concerns the analysis of particle dissolution where cross-diffusion aspects and a relaxation of thermodynamic equilibrium, are incorporated. Further, the level-set method and moving grid method are analyzed as candidates to model particle growth. In this paper we only consider the moving grid method and a presentation of the level-set method.

1.3 Organization of the paper

The current paper does not aim at being mathematically rigorous but merely aims at being descriptive about the implications of the developed mathematics of these more complex models. First we formulate the mathematical models for particle dissolution in Section 2. Here a one-dimensional multi-component model and two-dimensional model is formulated. Section 2 ends with a brief description of the mathematical implications of the models. Section 3 starts with available self-similar solutions for the one-dimensional (multi-component) models. Next, the numerical methods to solve the one- and two-dimensional models are described. Section 4 deals with applications of the models to experimental and industrial set-ups. Finally, some concluding remarks about the work are given and ongoing research is indicated.

2 Models

2.1 Models for multi-component alloys

We consider a particle of a multi-component β phase surrounded by a “matrix” of phase α , of either uniform or non-uniform composition. The boundary between the β -particle and α -matrix is referred to as the interface. The metal is divided into representative cells in which a single particle of phase β dissolves in an α -matrix. Particle dissolution is assumed to proceed by a number of subsequent steps [1, 23]: decomposition of the chemical bonds in the particle, crossing of the interface by atoms from the particle and long-distance diffusion in the α -phase. In the models of thermodynamic equilibrium, we assume in this section that the first two mechanisms proceed sufficiently fast with respect to long-distance diffusion and do not affect the dissolution kinetics. Hence, the interfacial concentrations are those as predicted by thermodynamics (local equilibrium). In [24] we considered the dissolution of a stoichiometric particle in a ternary alloy. The hyperbolic relationship between the interfacial concentrations for ternary alloys is derived using a three-dimensional Gibbs space. For the case that the particle consists of n chemical elements apart from the atoms that form the bulk of the β -phase, a generalization to a n -dimensional Gibbs hyperspace has to be made. The Gibbs surfaces become hypersurfaces. We expect that similar consequences apply and that hence the hyperbolic relation between the interfacial concentrations remains valid for the general stoichiometric particle in a multi-component alloy. We denote the chemical species by Sp_i , $i \in \{1, \dots, n + 1\}$. We denote the stoichiometry of the particle by $(Sp_1)_{m_1}(Sp_2)_{m_2}(Sp_3)_{m_3}(\dots)(Sp_n)_{m_n}$. The numbers m_1, m_2, \dots are stoichiometric constants. We denote the interfacial concentration of species i by c_i^{sol} and we use the following hyperbolic relationship for the interfacial concentrations:

$$f(c_1^{\text{sol}}, c_2^{\text{sol}}, \dots, c_n^{\text{sol}}) = (c_1^{\text{sol}})^{m_1}(c_2^{\text{sol}})^{m_2}(\dots)(c_n^{\text{sol}})^{m_n} - K_{\text{sol}} = 0, \quad (1)$$

where $K_{\text{sol}} = K_{\text{sol}}(T)$.

The factor K_{sol} is referred to as the solubility product. It depends on temperature T according to an Arrhenius relationship. In principle, the model can handle any form of temperature dependence for the solubility product.

We denote the position of the moving interface between the β -particle and α -phase by $S(t)$. Consider a one-dimensional domain, i.e. there is one spatial variable, which extends from 0 up to M . Since particles dissolve simultaneously in the metal, the concentration profiles between consecutive particles may interact and hence soft-impingement occurs. This motivates the introduction of finitely sized cells over whose boundary there is no flux. For cases of low overall concentrations in the alloy, the cell size M may be large and the solution resembles the case where M is infinite. The latter case can be treated easily with (semi) explicit expressions. The spatial co-ordinate is denoted by r , $0 \leq S(t) \leq r \leq M$. The α -matrix where diffusion takes place is given by $\Omega(t) := \{r \in \mathbb{R} : 0 \leq S(t) \leq r \leq M\}$. The β -particle is represented by the domain $0 \leq r < S(t)$. Hence for each alloying element, we have for $r \in \Omega(t)$ and $t > 0$ (where t denotes time)

$$\frac{\partial c_i}{\partial t} = \sum_{j=1}^n \frac{D_{ij}}{r^a} \frac{\partial}{\partial r} \left\{ r^a \frac{\partial c_j}{\partial r} \right\}, \quad \text{for } i \in \{1, \dots, n\}. \quad (2)$$

Here D_{ij} and c_i respectively denote the (cross-)diffusion coefficients and the concentration of the species i in the α -rich phase. If $D_{ij} < 0$ for some $i \neq j$, then, the transport of element i is delayed by the presence of element j . For $D_{ij} > 0$, the opposite holds. Experiments with Differential Scanning Calorimetry by Chen *et al* [22] for Al-Si-Mg alloys indicate that disregarding cross-diffusion terms gives a good approximation. However, for some other alloys the full diffusion matrix should be taken into account. A physical motivation of the above partial differential equation is given by Kirkaldy and Young [25]. The geometry is planar, cylindrical and spherical for respectively $a = 0, 1$ and 2 . Let c_i^0 denote the initial concentration of each element in the α phase, i.e. we take as initial conditions (IC) for $r \in \Omega(0)$

$$(IC) \quad \begin{cases} c_i(r, 0) = c_i^0(r), & \text{for } i \in \{1, \dots, n\}, \\ S(0) = S_0. \end{cases}$$

At a boundary not being an interface, i.e. at M or when $S(t) = 0$, we assume no flux through it, i.e.

$$\frac{\partial c_i}{\partial r} = 0, \quad \text{for } i \in \{1, \dots, n\}. \quad (3)$$

Furthermore at the moving interface $S(t)$ we have the “Dirichlet boundary condition” c_i^{sol} for each alloying element. The concentration of element i in the particle is denoted by c_i^{part} , this concentration is fixed at all stages. This assumption follows from the constraint that the stoichiometry of the particle is maintained during dissolution in line with Reiso et al [14]. The dissolution rate (interfacial velocity) is obtained from a mass-balance. Summarized, we obtain at the interface for $t > 0$ and $i, j \in \{1, \dots, n\}$:

$$\begin{cases} c_i(S(t), t) = c_i^{\text{sol}}, \\ \frac{dS}{dt} = \sum_{j=1}^n \frac{D_{ij}}{c_i^{\text{part}} - c_i^{\text{sol}}} \frac{\partial c_j}{\partial r}(S(t), t) \end{cases} \implies \sum_{k=1}^n \frac{D_{ik}}{c_i^{\text{part}} - c_i^{\text{sol}}} \frac{\partial c_k}{\partial r} = \sum_{k=1}^n \frac{D_{jk}}{c_j^{\text{part}} - c_j^{\text{sol}}} \frac{\partial c_k}{\partial r}. \quad (4)$$

The right part of the above equations, which holds on $S(t)$, follows from local mass-conservation of the components. Above formulated problem falls within the class of Stefan-problems, i.e. diffusion with a moving boundary. Since we consider simultaneous diffusion of several chemical elements, it is referred to as a “vector-valued Stefan problem”. The unknowns in above equations are the concentrations c_i , interfacial concentrations c_i^{sol} and the interfacial position $S(t)$. All concentrations are non-negative. The model was analyzed in [26–28].

In the above formulation, it was assumed that the interface concentrations satisfy thermodynamic equilibrium. In the next section we will abandon this assumption, i.e. the interface reactions will be taken into account.

The influence of cross-diffusion is investigated in terms of a parameter study in [29] and in terms of self-similar solutions as exact solutions for the unbounded domain in [26]. An numerical analysis of cross-diffusion controlled particle dissolution is presented in [27]. An application to Al-Cu-Mg alloys of this type of model was presented by Vusanovic and Krane [30]. Furthermore, some models for multi-component solid-state phase transformations, based on more thermodynamic considerations, have been presented in [9, 11, 20, 31].

For a mathematical overview of Stefan problems we refer to the textbooks of Crank [6], Chadam and Rasmussen [32] and Visintin [33].

2.2 Two dimensional models for binary alloys

In this section we consider a particle in a binary alloy in two spatial dimensions. Further, we take interfacial reactions as additional rate determining processes into account. To highlight the effect of the geometry and the interfacial reaction on dissolution kinetics we drop the multi-component approach and consider the simple case of a binary α - β alloy with a β particle. The initial concentration of β in the α -rich phase is equal to c^0 (mol/m³), whereas c^{part} denotes the concentration of β in the particle. The equilibrium β concentration in the alloy is c^{sol} ($c^{\text{part}} > c^{\text{sol}} > c^0$). When the temperature is increased, dissolution of the β -particle sets in.

In the 2D-model we use the geometry as given in Fig. 1. The domain filled

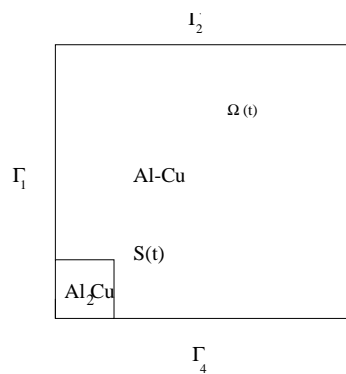


Fig. 1. Geometry of an β particle in Aluminum.

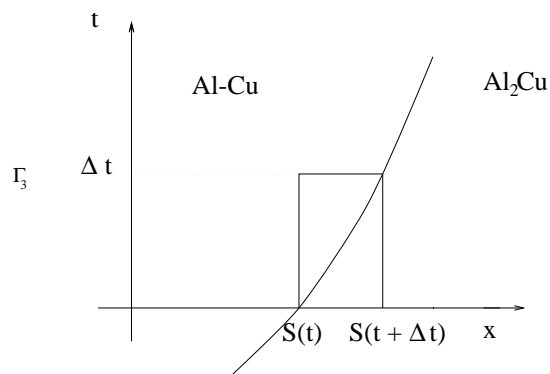


Fig. 2. The control volume.

with the α -rich phase is denoted by $\Omega(t)$. The boundary of this domain consists of the interface $S(t)$ and the outer boundaries Γ_i , $i \in \{1, 2, 3, 4\}$. The outer boundaries are fixed in time, except the intersections of Γ_1 and Γ_4 with $S(t)$. In the α -rich phase $\Omega(t)$, the β concentration $c(x, y, t)$ satisfies the (linear) diffusion equation

$$\frac{\partial c}{\partial t} = \mathbb{D} \Delta c, \quad (x, y) \in \Omega(t), \quad t \in (0, T]. \quad (5)$$

The diffusion coefficient \mathbb{D} (m²/s) is supposed to be independent of concentration.

As the initial condition we use

$$c(x, y, 0) = c^0(x, y), \quad (x, y) \in \Omega(0), \quad (6)$$

where $\Omega(0)$ is prescribed. We assume no flux of β atoms through the outer boundaries, so

$$\frac{\partial c}{\partial \mathbf{n}}(x, y, t) = 0, \quad (x, y) \in \Gamma_i, \quad i \in \{1, 2, 3, 4\}, \quad t \in [0, T]. \quad (7)$$

To determine the position of the interface two conditions are necessary. To derive these conditions for a spatially three dimensional problem, we consider a small part of the interface. Suppose that the interface is smooth, which means that it can locally be described by differentiable functions. For a small time step Δt the interface moves in the direction perpendicular to the interface. The x -axis is chosen along the normal. With this choice the position of the interface is locally described by the relation $x = S(t)$. We consider a control volume of width Δy and Δz . The intersection of the control volume with the surface $y = 0, z = 0$ is shown in Fig. 2. The balance of β atoms leads to the following equation (Stefan condition):

$$\begin{aligned} & (S(t + \Delta t) - S(t)) \Delta y \Delta z \cdot c^{\text{part}} \\ &= \mathbb{D} \frac{\partial c}{\partial x} \Delta y \Delta z \Delta t + (S(t + \Delta t) - S(t)) \Delta y \Delta z \cdot c^S, \end{aligned} \quad (8)$$

where c^S is the limit of the concentration in $\Omega(t)$ in the neighborhood of the interface. The left-hand side of (8) is equal to the amount of atoms transferred from the particle to the alloy. Assuming a first order reaction at the interface the second equation is (Robbins condition):

$$\begin{aligned} & K_{int} (c^{\text{sol}} - c^S) \Delta y \Delta z \Delta t \\ &= \mathbb{D} \frac{\partial c}{\partial x} \Delta y \Delta z \Delta t + (S(t + \Delta t) - S(t)) \Delta y \Delta z \cdot c^S, \end{aligned} \quad (9)$$

where K_{int} (m/s) is a measure of the rate of the interface reaction. For K_{int} large the problem is diffusion controlled, whereas for K_{int} small the problem is reaction controlled. Dividing (8) and (9) by $\Delta y \Delta z \Delta t$ and taking the limit $\Delta t \rightarrow 0$ one

obtains

$$\begin{aligned} c^{\text{part}} v_n(x, y, t) &= \mathbb{D} \frac{\partial c}{\partial \mathbf{n}}(x, y, t) + c^S v_n(x, y, t), \quad (x, y) \in S(t), \quad t \in (0, T], \end{aligned} \quad (10)$$

$$\begin{aligned} K_{int}(c^{\text{sol}} - c^S) &= \mathbb{D} \frac{\partial c}{\partial \mathbf{n}}(x, y, t) + c^S v_n(x, y, t), \quad (x, y) \in S(t), \quad t \in (0, T]. \end{aligned} \quad (11)$$

where \mathbf{n} is the unit normal vector on the interface pointing outward with respect to $\Omega(t)$ and v_n is the normal velocity of the interface.

In the references [1], [23] and [34] comparable boundary conditions are used. We remark that in the thermodynamic models, merely based on chemical potentials, due to Svoboda *et al* [7] and Sietsma and van der Zwaag [35], non-equilibrium interface conditions have been used too. Though, the last-mentioned approaches are built on different equations to solve.

2.3 Consistency checks for the models

We require that the total mass of all chemical elements is constant in the whole dissolution cell, i.e. over $0 \leq r \leq M$. Further, let c_i^0 be constant over $\Omega(0)$, then for the case of one spatial co-ordinate, we have

$$\int_0^M c_i(r, t) r^a dr = c_i^{\text{part}} \frac{S_0^{a+1}}{a+1} + c_i^0 \frac{M^{a+1} - S_0^{a+1}}{a+1}.$$

Subtraction of $\int_0^M c_i^0 r^a dr = c_i^0 \frac{M^{a+1}}{a+1}$ from both sides of above equation gives

$$\int_0^M (c_i(r, t) - c_i^0) r^a dr = (c_i^{\text{part}} - c_i^0) \frac{S_0^{a+1}}{a+1}. \quad (12)$$

All solutions of the Stefan-problem have to satisfy this condition. A mathematical theorem is rigorously proven in [36] also for multi-dimensional cases. We use an intuitive argument to show that some Stefan-problems do not have solutions that satisfy mass-conservation and hence are *ill-posed*.

Suppose that $c_i^0 < c_i^{\text{part}} < c_i^{\text{sol}}$, this situation is sketched in Fig. 3. Since from the maximum principle of the diffusion equation, it follows that extremes occur only at boundaries or at $t = 0$, the gradient must be negative, i.e. $\frac{\partial c_i}{\partial r}(S(t), t) < 0$. Since alloying elements diffuse from high concentration areas to low concentration areas, the alloying elements diffuse from the interface into the α -phase. Combination of $c_i^{\text{part}} - c_i^{\text{sol}} < 0$ and the rate-equation for the interface gives $\frac{dS}{dt} > 0$, i.e. the β -phase grows in the α -phase. This gives an increase of the concentration in the matrix of the alloying elements due to both growth ($c_i^{\text{part}} > c_i^0$) and to inward diffusion. This implies that the integral of the concentration, e.g. the total mass, is not constant. Hence a contradiction follows. This is shown in Fig. 3 where both the initial profile and a profile after a certain amount of time have been sketched.

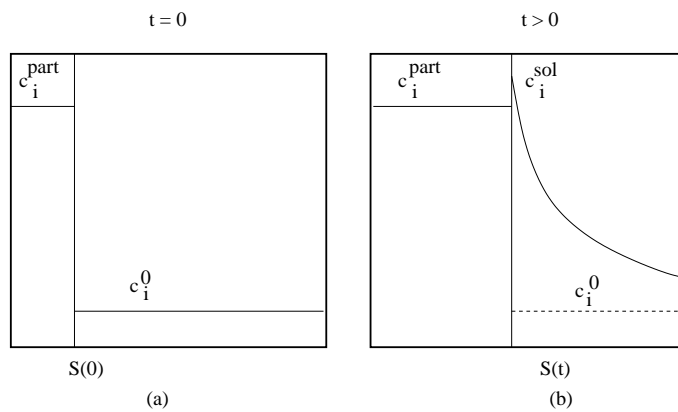


Fig. 3. The hypothetical case $c_i^0 < c_i^{\text{part}} < c_i^{\text{sol}}$ which gives growth of the α -phase and violation of the mass-balance. Left (a) shows the initial situation and right (b) shows a hypothetical (but impossible) situation at some time $t > 0$.

The following second argument also supports the above mentioned contradiction. Suppose that $c_i^0 < c_i^{\text{part}} < c_i^{\text{sol}}$, i.e. the interfacial concentration exceeds the initial concentration (see Fig. 3). From $t = 0$ the interfacial concentration can increase (build up) only due to transport of atoms from the particle to the interface and matrix (since concentration gradients and reactions are absent initially). This implies that the total number of atoms of the alloying elements in the particle must decrease. Since the concentration of the alloying elements in the particle is assumed to be constant, the particle must dissolve since alloying elements diffuse

from the particle into the matrix.

On the other hand from the maximum principle of the diffusion equation follows that $\frac{\partial c_i}{\partial r}(S(t), t) < 0$. Hence, the total number of atoms of the alloying element in the matrix increases. Furthermore, we have $c_i^{\text{part}} - c_i^{\text{sol}} < 0$, which implies $\frac{dS}{dt} > 0$, hence the total number of atoms of the alloying elements in the particle increases. This gives a contradiction with the remarks in the previous paragraph. Both the interfacial movement due to growth and the increase of the total number of atoms of the alloying element are sketched in Fig. 3. Mass can not be conserved for this case.

Similar arguments can be used to show that the other case $c_i^{\text{sol}} < c_i^{\text{part}} < c_i^0$ also violates mass-conservation (see Fig. 4). This statement can be generalized in

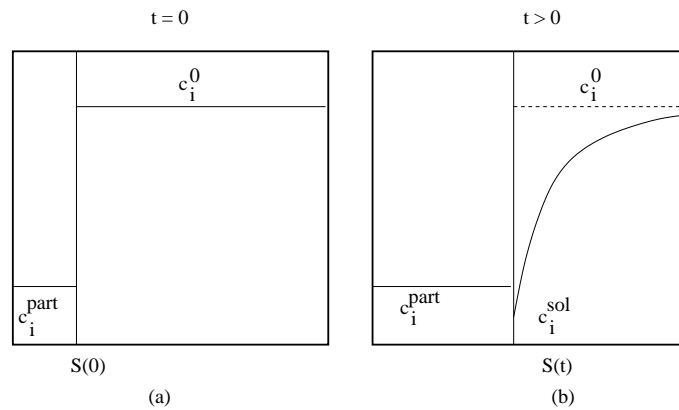


Fig. 4. The hypothetical case $c_i^{\text{sol}} < c_i^{\text{part}} < c_i^0$ which gives growth of the α -phase and violation of the mass-balance. Left (a) shows the initial situation and right (b) shows a hypothetical (but impossible) situation at some time $t > 0$.

the following result:

Theorem. *Let all concentrations be non-negative, then the following combinations give non-conserving solutions in the sense of equation (12):*

- (i) $c_i^{\text{sol}} < c_i^{\text{part}} < c_i^0$,
- (ii) $c_i^0 < c_i^{\text{part}} < c_i^{\text{sol}}$ (see Figs. 3, 4 for both cases).

This result is used to reject possible (numerical) unphysical solutions that result from the vector-valued Stefan problem. The theorem is proven in mathema-

tically rigorous way in [36]. Furthermore, negative concentrations are unphysical and hence rejected.

3 Solution procedures

3.1 Self-similar solutions and asymptotic approximations

We start this section by giving the self-similarity solution for the one-component problem. Subsequently, we give the self-similarity solution for the multi-component problem.

3.1.1 The binary alloy problem

Suppose that the interface concentration of a certain component is known, say $c(S(t), t) = c^{\text{sol}}$. Then, we have to solve the following problem (we refer to this problem as (P1)):

$$(P1) \quad \begin{cases} \frac{\partial c}{\partial t} = D \frac{\partial^2 c}{\partial r^2}, \\ \frac{dS}{dt} = \frac{D}{c^{\text{part}} - c^{\text{sol}}} \frac{\partial c}{\partial r}(S(t), t), \\ c(S(t), t) = c^{\text{sol}}, \\ c(r, 0) = c^0 = c(\infty, t), \quad S(0) = S_0. \end{cases}$$

As in [36] we search a self-similar solution for the function $c = c(r, t)$ and for $S = S(t)$. Trial of $c = c\left(\frac{r-S_0}{2\sqrt{Dt}}\right)$ shows that these expressions satisfy the differential equations in (P1). Setting $\eta := \frac{r-S_0}{2\sqrt{Dt}}$ gives an ordinary differential equation for $c = c(\eta)$. Substitution of $c(S(t), t) = c^{\text{sol}}$, solution of the ordinary differential equation and use of the initial condition gives

$$c(r, t) = \frac{c^0 - c^{\text{sol}}}{\text{erfc}\left(\frac{k}{2\sqrt{t}}\right)} \text{erfc}\left(\frac{r - S_0}{2\sqrt{Dt}}\right) + c^0.$$

The procedure to obtain the above result can be found in [36] or [29]. For the interface rate constant k one substitutes the relation $S = S_0 + k\sqrt{t}$ into equation (4).

$$\frac{c^0 - c^{\text{sol}}}{c^{\text{part}} - c^{\text{sol}}} \cdot \sqrt{\frac{D}{\pi}} \cdot \frac{e^{-\frac{k^2}{4D}}}{\text{erfc}\left(\frac{k}{2\sqrt{D}}\right)} = \frac{k}{2} \quad (13)$$

above equation is solved for k using a standard zero-point iteration method.

3.1.2 A self-similar solution for the multi-component problem

In this section we only treat the case without cross-diffusion, i.e. $D_{ij} = 0$ for $i \neq j$ and we define $D_{ii} =: D_i$. The solutions that are presented here can be extended for cross-diffusion using a diagonalization or Jordan form for the diffusion matrix. This is done in [26]. As a trial solution for the planar case in a semi-unbounded region, we take the interfacial concentrations to be constant (these concentrations are not constant in time for other cases). Equation (4) has to be fulfilled, hence combined with equation (13) one obtains the following system of non-linear equations to be solved for k and c_i^{sol} for $i \in \{1, \dots, n\}$:

$$\begin{cases} \frac{c_i^0 - c_i^{\text{sol}}}{c_i^{\text{part}} - c_i^{\text{sol}}} \cdot \sqrt{\frac{D_i}{\pi}} \cdot \frac{e^{-\frac{k^2}{4D_i}}}{\text{erfc}\left(\frac{k}{2\sqrt{D_i}}\right)} = \frac{k}{2}, & \text{for } i \in \{1, \dots, n\}, \\ (c_1^{\text{sol}})^{m_1} (c_2^{\text{sol}})^{m_2} (c_3^{\text{sol}})^{m_3} (\dots) = K_{\text{sol}}. \end{cases} \quad (14)$$

Using the assumption $\left| \frac{c_i^{\text{sol}} - c_i^0}{c_i^{\text{part}} - c_i^{\text{sol}}} \right| \ll 1$, This gives the following set of equations to be solved in $k, c_1^{\text{sol}}, c_2^{\text{sol}}, \dots, c_n^{\text{sol}}$.

$$\begin{cases} k = 2 \frac{c_i^0 - c_i^{\text{sol}}}{c_i^{\text{part}} - c_i^{\text{sol}}} \cdot \sqrt{\frac{D_i}{\pi}}, & \text{for } i \in \{1, \dots, n\}, \\ (c_1^{\text{sol}})^{m_1} (c_2^{\text{sol}})^{m_2} (c_3^{\text{sol}})^{m_3} (\dots) = K_{\text{sol}}. \end{cases} \quad (15)$$

The solution of (15) approximates the solution of (14) for $\left| \frac{c_i^{\text{sol}} - c_i^0}{c_i^{\text{part}} - c_i^{\text{sol}}} \right| \ll 1$.

The dilute case. We consider the case that the particle concentration is much larger than the interface concentration. Furthermore, we assume that the initial concentration in the matrix is almost equal to zero, i.e. $c_i^{\text{part}} \gg c_i^{\text{sol}} \gg c_i^0 \approx 0$. From the upper and lower bounds in the above expression, it follows that the interface velocity can be approximated by

$$\frac{dS}{dt} = -\frac{c_i^{\text{sol}}}{c_i^{\text{part}}} \sqrt{\frac{D_i}{\pi t}}, \quad \text{for } i \in \{1, \dots, n\}. \quad (16)$$

Since this has to hold for all $i \in \{1, \dots, n\}$ it follows that all interfacial concentrations can be expressed in terms of, for instance, the interfacial concentration corresponding to the first element, i.e.

$$-\frac{c_i^{\text{sol}}}{c_i^{\text{part}}} \sqrt{D_i} = -\frac{c_1^{\text{sol}}}{c_1^{\text{part}}} \sqrt{D_1} \implies c_i^{\text{sol}} = \frac{c_i^{\text{part}}}{c_1^{\text{part}}} \sqrt{\frac{D_1}{D_i}} \cdot c_1^{\text{sol}}.$$

We substitute all these expressions for c_i^{sol} into the hyperbolic relation for the interfacial concentrations (equation (1)) to obtain a simple exponential equation for c_1^{sol} whose non-negative real-valued solution gives

$$\begin{aligned} (c_1^{\text{sol}})^\mu \cdot \left(\frac{c_2^{\text{part}}}{c_1^{\text{part}}} \sqrt{\frac{D_1}{D_2}} \right)^{m_2} \cdot \left(\frac{c_4^{\text{part}}}{c_1^{\text{part}}} \sqrt{\frac{D_1}{D_4}} \right)^{m_4} \cdots \left(\frac{c_n^{\text{part}}}{c_1^{\text{part}}} \sqrt{\frac{D_1}{D_n}} \right)^{m_n} &= K_{\text{sol}} \\ \iff c_1^{\text{sol}} &= \frac{c_1^{\text{part}}}{\sqrt{D_1}} \left[\prod_{i=1}^n \left(\frac{\sqrt{D_i}}{c_i^{\text{part}}} \right)^{m_i} \cdot K_{\text{sol}} \right]^{\frac{1}{\mu}} \quad (\in \mathbb{R}^+), \end{aligned}$$

where $\prod_{i=1}^n f_i := f_1 f_2 \dots f_n$ and $\mu := m_1 + m_2 + \dots + m_n$. Note again that we consider only non-negative and real-valued concentrations. The solution for c_1^{sol} is substituted into (16) to obtain the interface velocity:

$$\begin{aligned} \frac{dS}{dt} &= -\frac{c_{\text{eff}}^{\text{sol}}}{c_{\text{eff}}^{\text{part}}} \sqrt{\frac{D_{\text{eff}}}{\pi t}}, \\ c_{\text{eff}}^{\text{sol}} &:= K_{\text{sol}}^{\frac{1}{\mu}}, \quad c_{\text{eff}}^{\text{part}} := \left[\prod_{i=1}^n (c_i^{\text{part}})^{m_i} \right]^{\frac{1}{\mu}}, \quad D_{\text{eff}} := \left[\prod_{i=1}^n (D_i)^{m_i} \right]^{\frac{1}{\mu}}. \end{aligned} \tag{17}$$

We see that for this case particle dissolution in a multi-component alloy is mathematically reduced to particle dissolution in a binary alloy. The effective parameters (particle concentration and diffusion coefficient) are equal to geometric averages with weights according to stoichiometry. For the details on the derivation as well as the solution for the dissolution of a spherical particle we refer to [29]. The case where equation (2) is extended with cross-diffusion terms is analyzed in [29] and [26]. In these papers a solution of the same nature has been obtained and applied.

3.2 Numerical procedures

In the literature one can find various numerical methods to solve Stefan problems. These methods can be distinguished in the following categories: front-tracking,

front-fixing and fixed-domain methods. In a front-fixing method a transformation to body fitted curvilinear coordinates is used (a special case is the Isotherm Migration Method (IMM) [6]). A drawback is that such a transformation can only be used for a relatively simple geometry. Fixed-domain methods are the enthalpy method (EM), and the variational inequality method (VI). In these methods a new unknown is introduced, which is the integral of the primitive variable. The free boundary is implicitly defined by this unknown. Since in our approach the equations hold for the concentration and there are no energies involved in the model, the enthalpy method and phase-field method are not used. We refer to [37] and [38] among others where the phase-field method is used to compute the solution of the moving boundary problem. An other recent method where the free boundary is implicitly defined is the level-set method as described by Chen *et al* [39] for Stefan problems. Here the interface is identified by the zero level-set of a marker function. The advantages of this method is that topological changes, such as breaking up, of the dissolving or growing phases are dealt with easily. On the other hand, since both the interfacial velocity and interfacial concentrations are here determined by the concentration gradient, a grid grid-refinement near the free boundary can be attractive. This implies that the grid moves anyway and hence the benefits for the level-set method due to a fixed grid no longer apply. Though, the level-set method remains the best candidate due to the ability of dealing with changing topologies and because remeshing steps are not needed. The IMM and VI methods are only applicable when the interface is an equi-concentration line. However, in our application where either multi-component particles or interfacial reactions are taken into account, the interface is not an equi-concentration line. Hence, (IMM) and (VI) methods are no suitable candidates. Therefore we use a front-tracking method which has the added benefit that a first order reaction at the interface can be incorporated in the model. The moving grid method solves one partial differential equation only. The mesh is moved using an arbitrary Lagrangian Eulerian method. Here, the method is relatively cheap compared to the level-set method, where also a first order hyperbolic partial differential equation for the level set function has to be solved with a continuous extension of the interface velocity at each time-step. However, it is sometimes necessary to change the topology of the elements, then, the moving grid method requires a remeshing

step, which involves an expensive two dimensional interpolation step. This is a very expensive step in the moving grid method. Further, topological changes of growing and dissolving (for instance the disappearance) phases are hard to implement into moving mesh methods. For these cases the level-set method becomes more attractive. First some numerical methods for multi-component alloys are presented. These methods are given for one spatial co-ordinate only. Then, the moving grid method for 2D problems is presented and finally the level-set method is described for 2D and 2D cases. We refer to [27, 40, 41] for more details.

3.2.1 Numerical methods for multi-component alloys

In this work we only treat the case without cross-diffusion. For the numerical treatment of cross-diffusion, we refer to [27]. We start with a discretization of the one-dimensional multi-component model. Our main interest is to give an accurate discretization of the boundary conditions for this Stefan problem with one spatial co-ordinate. Here we use the classical moving grid method of Murray and Landis [42] to discretize the diffusion equations. In this paper we briefly describe the method, for more details we refer to [36].

Discretization of the interior region. We use an implicit finite difference method to solve the diffusion equation in the inner region. An explicitly treated convection term due to grid-movement is included. Since the magnitude of the gradient is maximal near the moving interface we use a geometrically distributed grid such that the discretization near the interface is fine and coarse farther away from the moving interface. Furthermore, we use a virtual grid-point near the moving boundary. The distance between the virtual node and the interface is chosen equal to the distance between the interface and the first grid-node. The resulting set of linear equations is solved using a tridiagonal matrix solver.

Discrete boundary conditions at the interface for local equilibrium. We define the discrete approximation of the concentration as $c_{i,k}^j$, where j , i and k respectively denote the time-step, the index of the chemical (alloying) element and gridnode. The virtual gridnode behind the moving interface and the gridnode at the interface respectively have indices $k = -1$ and $k = 0$. At the moving

interface, we obtain from discretization of (4)

$$\frac{D_i}{c_i^{\text{part}} - c_i^{\text{sol}}} \frac{c_{i,1}^{j+1} - c_{i,-1}^{j+1}}{2\Delta r} = \frac{D_{i+1}}{c_{i+1}^{\text{part}} - c_{i+1}^{\text{sol}}} \frac{c_{i+1,1}^{j+1} - c_{i+1,-1}^{j+1}}{2\Delta r}, \text{ for } j \in \{1, \dots, n-1\}.$$

Note that the concentration profile of each element is determined by the value of the interfacial concentration. Above equation can be re-arranged into a zero-point equation for all chemical elements. All interfacial concentrations satisfy the hyperbolic relation (1). Combination of all this, gives for $i \in \{1, \dots, n-1\}$

$$\begin{aligned} f_i(c_{i,0}^{j+1}, c_{i+1,0}^j) &:= D_i(c_{i,1}^{j+1} - c_{i,-1}^{j+1})(c_{i+1}^{\text{part}} - c_{i+1}^{\text{sol}}) \\ &\quad - D_{i+1}(c_{i+1,1}^{j+1} - c_{i+1,-1}^{j+1})(c_i^{\text{part}} - c_i^{\text{sol}}) = 0, \\ f_n(c_1^{\text{sol}}, \dots, c_n^{\text{sol}}) &:= (c_1^{\text{sol}})^{m_1} (c_2^{\text{sol}})^{m_2} (\dots) (c_n^{\text{sol}})^{m_n} - K_{\text{sol}} = 0. \end{aligned}$$

To approximate a root for the “vector-function” \mathbf{f} we use Newton’s method combined with discrete approximations for the non-zero entries in the first $n-1$ rows of the Jacobian matrix. The iteration is terminated when sufficient accuracy is reached. This procedure is explained in more detail in [36].

Adaptation of the moving boundary. The moving interface is adapted according to equation (4). In [43] the forward (explicit) Euler and Trapezoidal time integration methods are described and compared. It was found that the (implicit) Trapezoidal method was superior in accuracy. Furthermore, the iteration step to determine the interfacial concentrations is included in each Trapezoidal step to determine the interfacial position. Hence, the work per time-iteration remains the same for both time-integration methods. Therefore, the Trapezoidal rule is used to determine the interfacial position as a function of time. We terminate the iteration when sufficient accuracy is reached, i.e. let ε be the inaccuracy, then we stop the iteration when the inequality

$$\sum_{i=1}^n |c_i^{\text{sol}}(p+1) - c_i^{\text{sol}}(p)| + \frac{|S^{j+1}(p+1) - S^{j+1}(p)|}{S^{j+1} - M} < \varepsilon$$

holds. Here S^j denotes the discrete approximation of the interfacial position at time-step j . The integer p represents the iteration number during the determination of the interfacial concentrations and position.

3.2.2 Moving Finite Element Method with conservative boundary displacement

The mesh on which the diffusion equation is solved is adapted according to the movement of the interface. The algorithm for an infinite rate of reaction, i.e. the interface concentration equals the concentration c^{sol} , which is determined by Thermodynamics, can be described as follows. In each time-step we solve the ALE (Arbitrary Lagrangian Eulerian) convection-diffusion equation

$$\frac{Dc}{Dt} - \mathbb{D}\Delta c - \mathbf{u}_{\text{mesh}} \cdot \nabla c = 0, \quad (18)$$

with $\frac{Dc}{Dt}$ the so-called material derivative and $\mathbf{u}_{\text{mesh}} = \frac{\mathbf{x}(t+\Delta t) - \mathbf{x}(t)}{\Delta t}$ the mesh velocity.

After that, the boundary is updated according to

$$\mathbf{x}(t + \Delta t) = \mathbf{x}(t) + v_n \Delta t \mathbf{n} = \mathbf{x}(t) + \frac{\mathbb{D}}{c^{\text{part}} - c^{\text{sol}}} \frac{\partial c}{\partial \mathbf{n}} \Delta t \mathbf{n}. \quad (19)$$

The straight-forward way to update the free boundary is to compute the gradient of the concentration in the elements connected to the free boundary (normal_velocity method). Using an averaging procedure for the gradient as well as an averaging procedure to compute the normals in the vertices of the boundary, equation (19) can be evaluated.

However, in case of sharp corners this may lead to a strange behavior as is shown in Fig. 5. In order to get rid of this phenomenon we developed an algorithm based on the integral representation of the Stefan boundary condition. The flux through the element $(\mathbf{x}_{i-1}, \mathbf{x}_i)$ (Fig. 7) is approximately equal to:

$$\mathbb{D} \frac{\partial c}{\partial \mathbf{n}}(\mathbf{x}_{i-\frac{1}{2}}) l_i \Delta t, \quad (20)$$

with l_i the length of the line element $(\mathbf{x}_{i-1}, \mathbf{x}_i)$. Hence the amount of diffused material through the boundary $(\mathbf{x}_{i-\frac{1}{2}}, \mathbf{x}_{i+\frac{1}{2}})$ is equal to

$$\frac{\Delta t}{2} \left(\mathbb{D} \frac{\partial c}{\partial \mathbf{n}}(\mathbf{x}_{i-\frac{1}{2}}) l_i + \mathbb{D} \frac{\partial c}{\partial \mathbf{n}}(\mathbf{x}_{i+\frac{1}{2}}) l_{i+1} \right). \quad (21)$$

The amount M_s of material dissolved, is approximately equal to $(c^{\text{part}} - c^{\text{sol}})O$, where O is the area defined in Fig. 7. Due to the balance of atoms M_s must

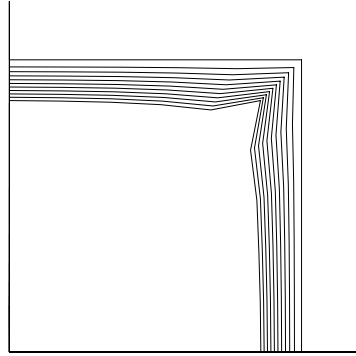


Fig. 5. Position of free boundary at first 10 time-steps using the normal velocity method for infinite rate of reaction.

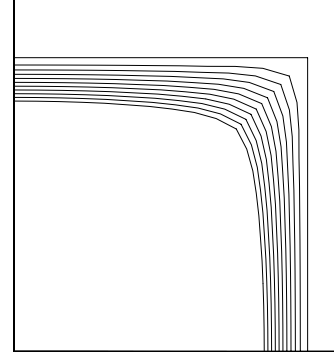


Fig. 6. Position of free boundary at first 10 time-steps using the Stefan method for infinite rate of reaction.

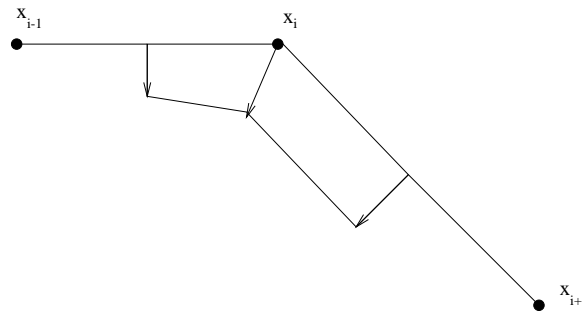


Fig. 7. Area occupied by the region defined by the displacement of the vertex.

be equal to the amount of diffused material given in equation (21). Consider two adjacent line elements $(\mathbf{x}_{i-1}, \mathbf{x}_i)$, and $(\mathbf{x}_i, \mathbf{x}_{i+1})$, with length l_i and l_{i+1} respectively (Fig. 7). The mid-side points of these elements are denoted by $\mathbf{x}_{i-\frac{1}{2}}$ and $\mathbf{x}_{i+\frac{1}{2}}$. Let the from formula (19) computed displacement in the mid-side points, be equal to $\delta x_{i-\frac{1}{2}}$ and $\delta x_{i+\frac{1}{2}}$. The new position of vertex \mathbf{x}_i is denoted by $\hat{\mathbf{x}}_i$. The vector $\hat{\mathbf{x}}_i - \mathbf{x}_i$ is parallel to the average of the normal vectors on the line elements $(\mathbf{x}_{i-1}, \mathbf{x}_i)$ and $(\mathbf{x}_i, \mathbf{x}_{i+1})$. The length of the displacement given by $\Delta x_i = \|\hat{\mathbf{x}}_i - \mathbf{x}_i\|$ is such that $M_s = (c^{\text{part}} - c^{\text{sol}})O$. Once the displacement in the vertices is computed, also the displacements in the mid-side points change. In order to get both a local and global equilibrium in the amount of dissolved

material, it is necessary, that the new area is equal to $M_s/(c^{\text{part}} - c^{\text{sol}})$. The area O depends on Δx_i , $\Delta x_{i-\frac{1}{2}}$ and $\Delta x_{i+\frac{1}{2}}$, where $\Delta x_{i-\frac{1}{2}}$ is the adapted length of the displacement in $\mathbf{x}_{i-\frac{1}{2}}$. Since $\Delta x_{i-\frac{1}{2}}$ and $\Delta x_{i+\frac{1}{2}}$ depend on Δx_{i-1} , Δx_i and Δx_{i+1} the relation is non-linear.

To solve this non-linear system we had to use an under-relaxation parameter. Choosing this parameter equal to 0.5 gives a fast convergence. The results of the Stefan algorithm are shown in Fig. 6. The results in Fig. 6 are more reliable than those in Fig. 5 since from physical point of view we expect a large diffusion of the atoms at the angular free boundary point. This gives locally larger free boundary velocities. For more details we refer to [40]. For the implementation of a finite rate of the interface reactions, more details can be found in [44].

3.2.3 Level-Set method for Stefan problem

In this section we summarize the main principles of the Level-Set method for the dissolution or growth of particles applied to the problem in the previous section. The method was introduced by Osher and Sethian [45] and the method has a wide applicability in problems with moving interfaces, see Sethian [46]. Some of these problems, among others, are bubbly flows [47], phase transformations [39] and particle dissolution [18]. A recent book on the topic is due to Osher and Fedkiw [48].

The main principle is that the Level-Set method captures the zero level of a continuous function $\phi = \phi(\mathbf{x}, t)$, which is initialized as a signed distance function. This function, commonly referred to as the Level-Set function, is chosen to be positive in the diffusive phase and negative in the particle domain:

$$\phi(x, y, 0) = \begin{cases} +\text{dist}(\mathbf{x}, S(0)), & \text{if } \mathbf{x} \in \Omega(0), \\ 0, & \text{if } \mathbf{x} \in S(0), \\ +\text{dist}(\mathbf{x}, S(0)), & \text{if } \mathbf{x} \notin \Omega(0) \cup S(0). \end{cases} \quad (22)$$

The movement of the interface is represented by using the Level-Set function by means of

$$\frac{\partial \phi}{\partial t} + v_n \|\nabla \phi\| = 0. \quad (23)$$

Here v_n denotes the normal velocity at the interface, which is computed by the use of the Stefan condition. This equation is valid at the interface only. The

above equation is extended over the entire domain of computation if the interface velocity is also extended continuously, to obtain

$$\frac{\partial \phi}{\partial t} + \mathbf{v} \cdot \nabla \phi = 0, \quad (24)$$

In general after advecting the interface using equation (24), the Level-Set function is no longer a distance function, which may lead to very small or large gradients of ϕ . This is not desirable for the computation of the curvature given by $\kappa = \nabla \cdot \mathbf{n}$ needed for the incorporation of the Gibbs-Thomson effect. Furthermore, the Level-Set function needs to be a continuous function since it is used to track the interface. Therefore, the Level-Set function is re-initialized by solving

$$\frac{\partial \psi}{\partial \tau} = \text{Sign}(\phi(x, t))(1 - \|\nabla \psi\|) \quad (25)$$

in pseudo-time τ with initial condition $\psi(\mathbf{x}, 0) = \phi(\mathbf{x}, t)$. This procedure was introduced by Sussman *et al* [49]. After this re-initialization step the normal vector is given by $\mathbf{n} = \nabla \phi$. The front velocity is extended continuously so that equation (24) can be solved over the entire domain of computation. The extension of \mathbf{v} is done in pseudo-time τ so that for each spatial co-ordinate, $q \in \{x, y, z\}$, we have

$$\begin{cases} \frac{\partial v_q}{\partial \tau} + \text{Sign}\left(\phi \frac{\partial \phi}{\partial q}\right) \frac{\partial v_q}{\partial q} = 0, \\ v_q(\mathbf{x}, 0) = \frac{D}{c^{\text{part}} - c^{\text{sol}}} \frac{\partial c}{\partial q}, \end{cases} \quad \mathbf{x} \in S(t), \quad \text{for } q \in \{x, y, z\}. \quad (26)$$

The diffusion equation for the concentration is presently solved by the use of Finite Elements in [41] and the Level-Set equation is solved by a finite difference method. The re-initialization step is done by the Godunov's scheme, use of a Runge-Kutta time integration and a WENO scheme for the spatial derivatives. The combination of these methods gives a TVD scheme. Details on the numerical solution of these equations can be found in, among others, [39] (fully Finite Differences) and [41] (combined Finite Differences and Finite Elements). It turns out that the Level-Set method handles three dimensional geometries and topologically

changing geometries more easily than the moving grid method does. Furthermore, the additional conservation argument that was necessary for the 2D moving finite element method (see the previous section and [40]), is no longer needed for the Level-Set method (see [41]). By Javierre *et al* [41] some 2D and 3D test-cases are shown with a dissolving radially perturbed cylinder, which breaks up into several rounded particles dissolving at different paces due the presence of each other.

4 Applications

4.1 Particle dissolution in multi-component alloys

In this section we consider particle dissolution in a multi-component alloy modelled with a one-dimensional model. First, we show a comparison between a full multi-component model and the quasi-binary model (see equation (15)). Subsequently, we compute dissolution of a particle in competition with a segregation at a grain boundary under a temperature-time profile. The latter case comes from an industrial application. All examples given here are hypothetical.

4.1.1 Comparison between multi-component computation and the quasi-binary solution for a planar case

The one-dimensional model of Section 2 is applied here for the dissolution of a particle in a multi-component alloy. The example concerns a planar geometry with three alloying elements with $c_i^{\text{part}} = 100$, $c_i^0 = 0$ and $D_i = i \cdot 10^{-13}$ for $i \in \{1, 2, 3\}$. Further, the solubility product $K_{\text{sol}} = 1$ and initial interfacial position $S(0) = 0.1 \cdot 10^{-6}$. Fig. 8 shows the interface position as a function of time. The curves have been obtained using the analytical approach (see the top curve of the analytical approaches in Fig. 8). From Fig. 8 it is clear that the analytical (multi-component and quasi-binary) approaches co-incide well at all times. At the early stages the analytical approaches co-incide well with the numerical solution. As time proceeds the numerical solution starts to deviate due to the finite size of the cell in which the particle dissolves (soft-impingement). For the same set of parameters we show concentration profiles of the three alloying elements in Fig. 9. The profiles were obtained using the numerical method from Section 3.

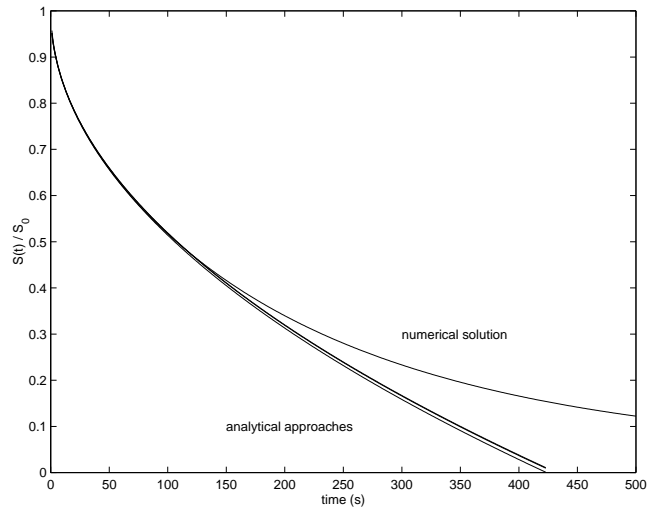


Fig. 8. The interface position as a function of time during the dissolution of a planar phase. The top curve represents the solution obtained by the Finite Difference method with an finite volume of the cell. The other curves represent the analytical approaches for the infinite volume of the cell, where the lowest curve represents the quasi-binary approach and the other curve represents the full multi-component “analytical” solution where a zero-point method is used.

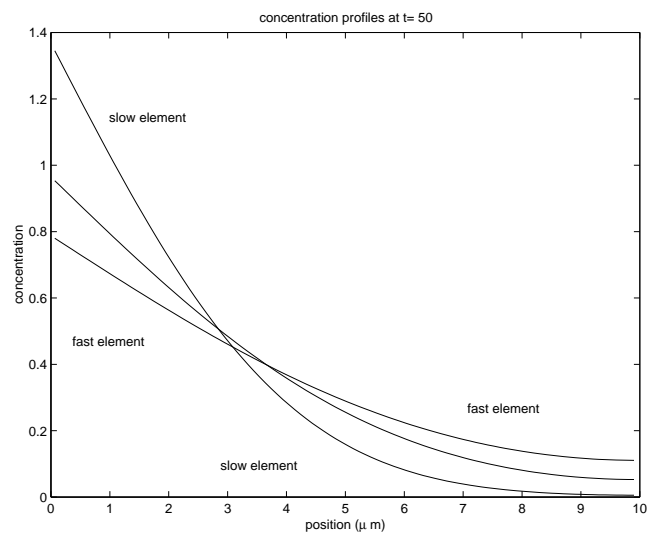


Fig. 9. Concentration profiles of the alloying elements at time $t = 50$.

4.1.2 Comparison between multi-component computation and the quasi-binary solution for a spherical case

Finally we show the dissolution of a spherical particle in a multi-component alloy with three alloying elements. The initial particle size S_0 and cell size M are 10^{-6} m and 10^{-5} respectively. The other input-data are listed in Table 1.

Table 1. Input data

Physical quantity	Value	Si-Unit
D_1	10^{-13}	m^2/s
D_2	$2 \cdot 10^{-13}$	m^2/s
K_{sol}	1	–
c_1^{part}	33	–
c_2^{part}	33	–
c_i^0	0	–
m_1	1	–
m_2	2	–

In [29] we developed a quasi-binary approach for spherical geometries. The results for the quasi-binary approach, as derived in [29], are compared to the “exact” full multi-component solution, which has also been derived there. We distinguish various cases where c_3^{part} and D_3 are varied and all other parameters are fixed as in Table 1. The following cases are shown in Fig. 10:

- $c_3^{\text{part}} = 33 = c_1^{\text{part}} = c_2^{\text{part}}$, $D_3 = 0.1 \cdot 10^{-13} \ll D_1, D_2$ (curve I);
- $c_3^{\text{part}} = 3 \ll c_1^{\text{part}}, c_2^{\text{part}}$, $D_3 = 0.1 \cdot 10^{-13} \ll D_1, D_2$ (curve II);
- $c_3^{\text{part}} = 33 = c_1^{\text{part}} = c_2^{\text{part}}$, $D_3 = 10 \cdot 10^{-13} \gg D_1, D_2$ (curve III);
- $c_3^{\text{part}} = 3 \ll c_1^{\text{part}} = c_2^{\text{part}}$, $D_3 = 10 \cdot 10^{-13} \gg D_1, D_2$ (curve IV).

From Fig. 10 it is clear that the quasi-binary approach co-incides well with the full multi-component approach, especially when the third alloying element diffuses fast. So the quasi-binary approach is a handy tool to give a fast estimate for the order of magnitude of the dissolution time.

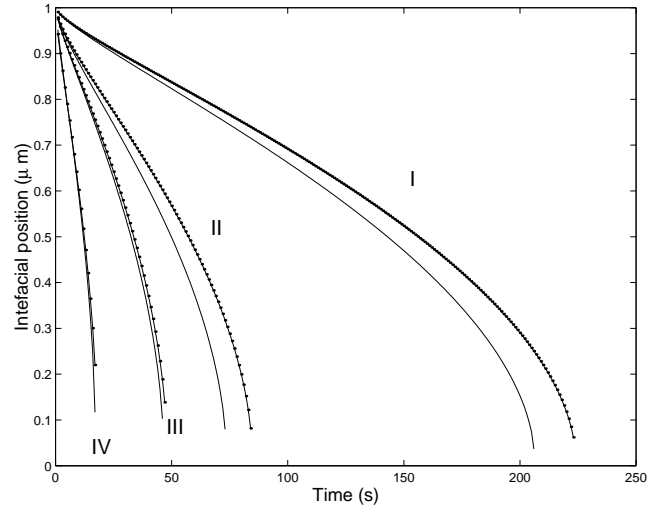


Fig. 10. The interfacial position as a function of time. All curves correspond to the configuration as listed in Table 1. The bold and ordinary curves respectively reflect the quasi-binary and full multi-component solution. Curves I corresponds to $c_3^{\text{part}} = 33$ and $D_3 = 0.1 \cdot 10^{-13}$. Curve II reflects the case that $c_3^{\text{part}} = 3$ and $D_3 = 0.1 \cdot 10^{-13}$. Curve III displays the situation in which $c_3^{\text{part}} = 33$ and $D_3 = 10 \cdot 10^{-13}$, whereas curve IV shows the configuration $c_3^{\text{part}} = 3$ and $D_3 = 10 \cdot 10^{-13}$.

4.1.3 A simultaneously dissolving particle at the center and a segregation at the grain boundary

We consider a hypothetical industrial application where simultaneous dissolution of a Si-particle and Mg_2Si -segregation at the grain boundary is modelled under a temperature that depends on time. The initial temperature is set at 300 K, heat-up rate 0.05 K/s and the homogenization temperature is set at 833 K. Further, the initial concentrations are $c_{\text{Mg}}^0 = 0.04$, $c_{\text{Si}}^0 = 0$ with particle concentrations $c_{\text{Si}}^{\text{part}} = 35$, $c_{\text{Mg}}^{\text{part}} = 65$ in the segregation at the grain boundary. The geometry is shown in Fig. 11. The size of the Si-particle and Mg_2Si -segregation is shown in Fig. 12. In the example the dimensions were chosen such that the Mg_2Si -segregation dissolves completely and the Si-particle only partly due to Si-accumulation in the matrix.

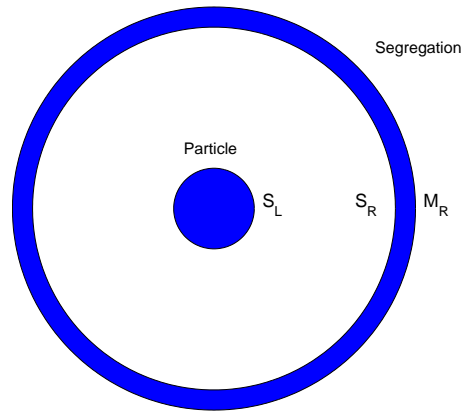


Fig. 11. The geometry of a grain with a Si-particle in the center and a Mg_2Si -segregation at the grain boundary.

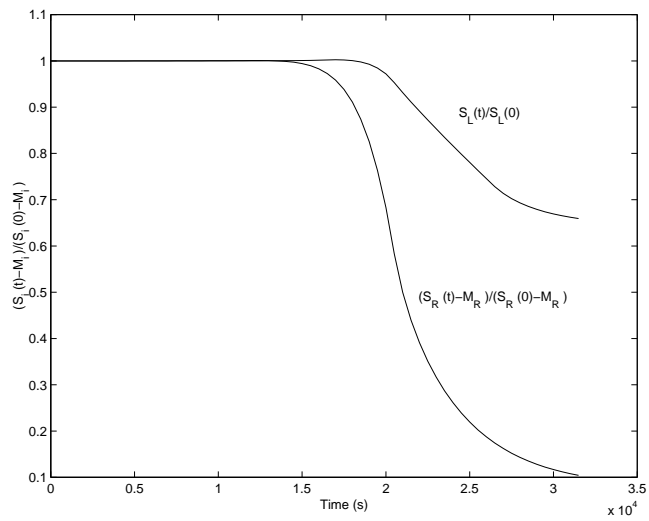


Fig. 12. The evolution of the particle and size of the segregation during the homogenization process.

4.2 Numerical experiments with the interface reaction for two dimensions

An algorithm has been developed to investigate the dissolution kinetics for a two-dimensional case with a first order reaction at the interface. This algorithm has been implemented in our finite element code SEPRAN [50]. As an example we consider the dissolution of a needle shaped particle in a bar. Due to the symmetry of this two-dimensional problem, we restrict the simulation to one quarter of the real geometry. First we investigate the influence of the rate of the interface reaction (K_{int}) on the shape of the dissolving particle. Thereafter we compare the influence of the extra terms used in (10) and (11). In all our examples we have chosen the following parameters:

$$\begin{array}{ll} \text{diffusion coefficient} & \mathbb{D} = 0.04858, \\ \text{concentration in the particle} & c^{part} = 54, \\ \text{initial concentration} & c^0 = 0.0011. \end{array}$$

4.2.1 The influence of the interface reaction

We consider a square dissolving in a square for various choices of K_{int} . The Figs. 13, 14 contain the results for $K_{int} = 1000$, and 0.1. For K_{int} large we expect that the solution converges to the solution of the Dirichlet problem. When the grid is refined we observe that the Dirichlet solution converges to the solution

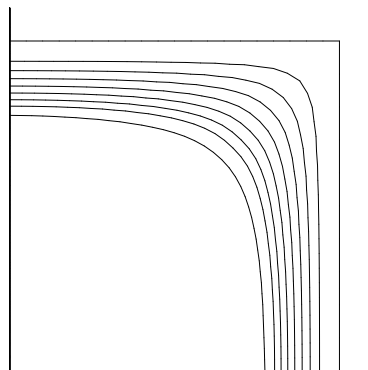


Fig. 13. Free boundary of a bar dissolving in a bar with $K_{int} = 1000$ and $c^{sol} = 3.88$.

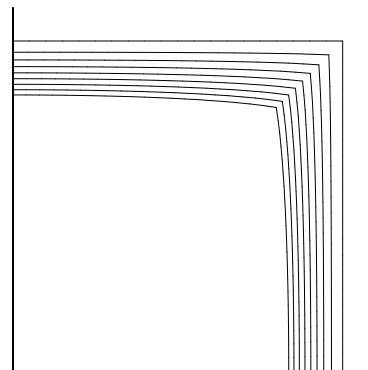


Fig. 14. Free boundary of a bar dissolving in a bar with $K_{int} = 0.1$ and $c^{sol} = 3.88$.

as given in Fig 13.

For small values of K_{int} the evolution of the position of the interface is completely determined by the rate of the interface reaction. Therefore one expects that the particle remains square-like. This is in accordance with the results as given in Fig. 14. For more details and experiments, we refer to [44]. Also the velocity of the interface decreases when K_{int} decreases.

4.2.2 The influence of the term $c^S v_n$

In the derivation of the model we have already noted that in some references the term $c^S v_n$ is deleted from equation (11). For the problem as considered in Section 4.2.1 we have compared the solution with and without this term and it appears that its influence is negligible. On the other hand when c^{sol} is closer to c^{part} the differences may be large. Therefore we consider an academic problem where c^{sol} is 10 times as large (see Fig. 15, 16). The results of the correct boundary conditions are given in Fig. 15. Since c^{sol} is much larger the velocity of the

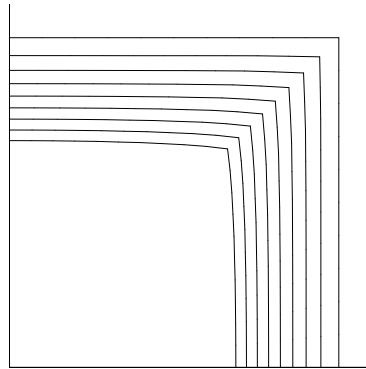


Fig. 15. Free boundary of a bar dissolving in a bar with $K = 0.1$ and $c^{sol} = 38.8$

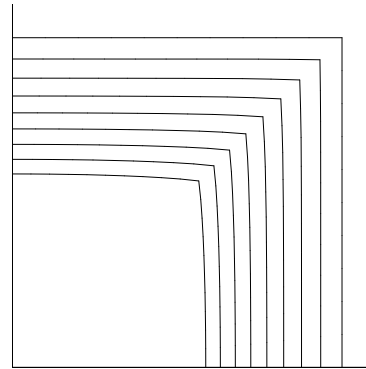


Fig. 16. Free boundary of a bar dissolving in a bar with $K = 0.1$ and $c^{sol} = 38.8$ without the term $c^S v_n$

interface is much higher. Therefore the time-steps used in these problems are equal to the time-steps of the previous problem divided by 10. The results given in Fig. 16 are obtained when the term $c^S v_n$ is deleted from equation (11). There are considerable differences between both results. Neglecting $c^S v_n$ leads to an overestimate of the position of the free boundary.

4.3 3D topological changes by the Level-Set method

To illustrate the power of the Level-Set method for three spatial dimensions, we consider a hypothetical dissolving particle that was dumbbell-shaped initially (see Fig. 17). The dumbbell is placed in a cubic domain of $[-5,5]^3$ with 33 gridpoints in each spatial direction. The interface concentration is given by $c^{\text{sol}} = 0.35$, particle concentration $c^{\text{part}} = 0.53$ and initial concentration $c^0 = 0.3$. The diffusivity is taken $D = 1$. These numbers are fully hypothetical and can be scaled in micrometers, which is the physical size of the problem that we consider here. In the early stages the topology does not change (see Fig. 18). As time proceeds, the dumbbell splits up into two parts (see Fig. 19), which will dissolve entirely in this configuration. If the moving mesh method were used, then, the computer code should contain various if-statements to deal with the splitting into two particles and with dissolving of either of the particles. The Level-Set method handles this in a more natural way.

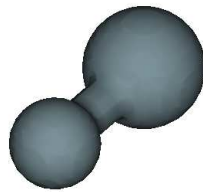


Fig. 17. Initial dumbbell shape of a hypothetical dissolving particle.

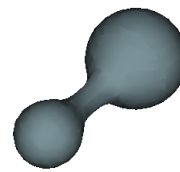


Fig. 18. Dumbbell shape of a hypothetical dissolving particle after some short time.



Fig. 19. Dissolving particles resulting due to splitting of the dumbbell at a later stage.

5 Conclusion and current work

Summarized, recently the following improvements have been achieved in modeling particle dissolution in alloys:

- Mathematical insight into the qualitative behavior of solutions of moving boundary problems associated with particle dissolution has been obtained. This insight provides quick analytical solutions and solution bounds, which are motivated by rigorous mathematical arguments. Further, approximate solutions have been obtained for modeling dissolution of particles in multi-component alloys.
- Numerical solution techniques to accomplish particle dissolution in multi-component alloys have been obtained.
- Further, a two-dimensional Finite Element method, based on a moving grid method, has been developed where the Stefan condition is discretized such that mass is conserved.
- Recently, the one-dimensional multi-component model has been extended to include effects from cross-diffusion. Metallurgical implications have been described in [29]. A mathematically rigorous analysis has been given in [26–28].
- Recently, the Level-Set method is successfully applied to the dissolution problem with 2 and 3 spatial dimensions. The Level-Set method enables us to deal with splitting of dissolving phases. This method will be extended to multi-component alloys, i.e. vector-valued Stefan problems.

References

1. F. V. Nolfi jr., P.G. Shewmon, J.S. Foster. The dissolution and growth kinetics of spherical particles, *Transactions of the Metallurgical Society of AIME*, **245**, pp. 1427–1433, 1969.
2. M. J. Whelan. On the kinetics of particle dissolution, *Metals Science Journal*, **3**, pp. 95–97, 1969.

3. U. L. Baty, R. A. Tanzilli, R. W. Heckel. Dissolution kinetics of CuAl_2 in an Al-4Cu alloy, *Metallurgical Transactions*, **1**, pp. 1651–1656, 1970.
4. U. H. Tundal, N. Ryum. Dissolution of particles in binary alloys: Part i: computer simulations, *Metallurgical Transactions*, **23A**, pp. 433–449, 1992.
5. H. B. Aaron, G. R. Kotler. Second phase dissolution, *Metallurgical Transactions*, **2**, pp. 1651–1656, 1971.
6. J. Crank. *Free and moving boundary problems*, Clarendon Press, Oxford, 1984.
7. J. Svoboda, F. D. Fischer, P. Fratzl, E. Gamsjäger, N. K. Simha. Kinetics of interfaces during diffusional transformations, *Acta Materialia*, **49**, pp. 1249–1259, 2001.
8. M. Hillert. *Phase equilibria, phase diagrams and phase transformations, their thermodynamic basis*, Cambridge University Press, Cambridge, 1998.
9. J. Ågren. Numerical treatment of diffusional reactions in multi-component alloys, *Journal of Physics and Chemistry of Solids*, **43**(4), pp. 285–391, 1982.
10. S. Crusius, G. Inden, U. Knoop, L. Höglund, J. Ågren. On the numerical treatment of moving boundary problems. *Zeitschrift für Metallkunde*, **83**, pp. 673–69, 1992.
11. J.-O. Andersson, J. Ågren. Models for numerical treatment of multicomponent diffusion in simple phases, *Journal of Applied Physics*, **72**(4), pp. 1350–1355, 1981.
12. J. M. Vitek, S. A. Vitek, S. A. David. Modelling of diffusion controlled phase transformation in ternary systems and application to the ferrite-austenite transformation in the Fe-Cr-Ni-system, *Metallurgical Transactions A*, **26A**, pp. 2007–2025, 1995.
13. R. Hubert. Modelisation numerique de la croissance et de la dissolution des precipites dans l'acier, *ATB Metallurgie*, **34–35**, pp. 4–14, 1995.
14. O. Reiso, N. Ryum, J. Strid. Melting and dissolution of secondary phase particles in AlMgSi-alloys, *Metallurgical Transactions A*, **24A**, pp. 2629–2641, 1993.
15. R. Kobayashi. Modeling and numerical simulations of dendritic crystal growth, *Physics D*, **63**, pp. 410–423, 1993.
16. E. Burman, M. Picasso, J. Rappaz. Analysis and computation of dendritic growth in binary alloys using a phase-field model, *Numerical Mathematics and Advanced Applications*, Springer, pp. 204–220, 2004.
17. U. Grafe, B. Böttger, J. Tiaden, S. G. Fries. Coupling of multicomponent thermodynamics to a phase field model: application to solidification and solid-state transformations of superalloys, *Scripta Materialia*, **42**, pp. 1179–1186, 2000.

18. E. Javierre, C. Vuik, F.J. Vermolen, S. van der Zwaag. A comparison of numerical models for one-dimensional stefan problems. *Journal of Computational and Applied Mathematics*, page accepted, 2005.
19. I. Kovacevic, B. Sarler. Solution of a phase-field model for dissolution of primary particles, *Conference of Advances of Solidification Processes in Stockholm*, 2005.
20. K. Thornton, J. Ågren, P. W. Voorhees. Modelling the evolution of phase boundaries in solids at the meso- and nano-scales, *Acta Materialia*, **51**, pp. 5675–5710, 2003.
21. F.J. Vermolen, H. M. Slabbekoorn, S. van der Zwaag. The apparent activation energy for the dissolution of spherical Si-particles in AlSi-alloys, *Materials Science and Engineering A*, **A231**, pp. 80–89, 1997.
22. S. P. Chen, M. S. Vossenbergh, F.J. Vermolen, J. van der Langkruis, S. van der Zwaag. Dissolution of β -particles in an Al-Mg-Si alloy during DSC runs, *Materials Science and Engineering A*, **A272**, pp. 250–256, 1999.
23. F.J. Vermolen, S. Van der Zwaag. A numerical model for the dissolution of spherical particles in binary alloys under mixed mode control, *Materials Science and Engineering A*, **220**, pp. 140–146, 1996.
24. F.J. Vermolen, C. Vuik, S. van der Zwaag. The dissolution of a stoichiometric second phase in ternary alloys: a numerical analysis, *Materials Science and Engineering*, **A246**, pp. 93–103, 1998.
25. J. S. Kirkaldy, D. J. Young. *Diffusion in the condensed state*, The Institute of Metals, London, 1987.
26. F.J. Vermolen, C. Vuik, S. van der Zwaag. Cross-diffusion controlled particle dissolution in metallic alloys, *Computing and Visualization in Science*, **8**, pp. 27–33, 2005.
27. F.J. Vermolen, C. Vuik. Solution of vector valued stefan problems with cross-diffusion, *Journal of Computational and Applied mathematics*, **176**(1), pp. 179–201, 2005.
28. F.J. Vermolen, C. Vuik. Numerical solution of vector-valued stefan problems. *Conference ECCOMAS 2004*, P. Neittaanmäki et al, (Eds.), Jyväskylä, Finland, 2004.
29. F.J. Vermolen, C. Vuik, S. van der Zwaag. Particle dissolution and cross-diffusion in multi-component alloys, *Materials Science and Engineering A*, **A347**, pp. 265–279, 2003.
30. I. Vusanovic, M. J. Krane. Microsegregation during solidification of Al-Cu-Mg alloys with varying composition, *International Communications in Heat and Mass Transfer*, **29**(3), pp. 1037–1046, 2002.

31. C. Atkinson, T. Akbay, R. C. Reed. Theory for reaustenization from ferrite-cementite mixtures in Fe-C-X steels, *Acta Metallurgica et Materialia*, **43**(5), pp. 2013–2031, 1995.
32. J. Chadam, H. Rasmussen. *Free boundary problems involving solids*, Longman, Scientific & technical, Harlow, 1993.
33. A. Visintin. *Models of phase transitions*, Progress in nonlinear differential equations and their application: 38 Birkhauser, Boston, 1996.
34. C. Vuik, C. Cuvelier. Numerical solution of an etching problem, *Journal of Computational Physics*, **59**, pp. 247–263, 1985.
35. J. Sietsma, S. van der Zwaag. A concise model for mixed-mode phase transformation in the solid state, *Acta Materialia*, **52**, pp. 4143–4152, 2003.
36. F.J. Vermolen, C. Vuik. A mathematical model for the dissolution of particles in multi-component alloys, *Journal of Computational and Applied Mathematics*, **126**, pp. 233–254, 2001.
37. M. Fabbri, V.R. Voller. The phase-field method in the sharp-interface limit: a comparison between models potentials, *Journal of Computational Physics*, **130**, pp. 256–265, 1997.
38. J. A. Mackenzie, M. L. Robertson. A moving mesh method for the solution of the one-dimensional phase-field equations, *Journal of Computational Physics*, **181**(2), pp. 526–544, 2002.
39. S. Chen, B. Merriman, S. Osher, P. Smereka. A simple Level-Set method for solving Stefan problems, *Journal of Computational Physics*, **135**, pp. 8–29, 1997.
40. A. Segal, C. Vuik, F.J. Vermolen. A conserving discretisation for the free boundary in a two-dimensional stefan problem, *Journal of Computational Physics*, **141**, pp. 1–21, 1998.
41. E. Javierre, C. Vuik, F.J. Vermolen, A. Segal. A Level Set Method for Particle Dissolution in a Binary Alloy, in progress, 2005.
42. W.D. Murray, F. Landis. Numerical and machine solutions of transient heat conduction problems involving freezing and melting, *Transactions ASME (C), Journal of Heat Transfer*, **245**, pp. 106–112, 1959.
43. F.J. Vermolen, C. Vuik. A numerical method to compute the dissolution of second phases in ternary alloys, *Journal of Computational and Applied Mathematics*, **93**, pp. 123–143, 1998.

44. C. Vuik, A. Segal, F.J. Vermolen. A conserving discretisation for a stefan problem with an interface reaction at the free boundary, *Computation and Visualisation of Science*, **3**, pp. 109–114, 2000.
45. S. Osher, J.A. Sethian. Fronts propagating with curvature-dependent speed: Algorithms based on hamilton-jacobi formulations, *Journal of Computational Physics*, **141**, pp. 12–49, 1988.
46. J. A. Sethian. *Level-Set methods and fast marching methods*, Cambridge University Press, New York, 1999.
47. S. P. van der Pijl, A. Segal, C. Vuik, P. Wesseling. A mass-conserving Level-Set method for modelling multi-phase flows, *International Journal of Numerical Methods in Fluids*, pp. 339–361, 2005.
48. S. Osher, R. Fedkiw. *Level-Set methods and dynamic implicit surfaces*, Springer-Verlag, New York, 2003.
49. M. Sussman, P. Smereka, S. Osher. A level-set approach for computing solutions to incompressible flow. *Journal of Computational Physics*, **114**, pp. 146–159, 1994.
50. A. Segal. *Sepran manuals*, 1984.